Phase equilibria in polydisperse nonadditive hard-sphere systems

Patrice Paricaud*
Laboratoire de Chimie et Procédés, ENSTA, ParisTech, 32 Bd Victor, 75739, Paris cedex 15, France
(Received 28 March 2008; published 14 August 2008)

Colloidal particles naturally exhibit a size polydispersity that can greatly influence their phase behavior in solution. Nonadditive hard-sphere (NAHS) mixtures are simple and well-suited model systems to represent phase transitions in colloid systems. Here, we propose an analytical equation of state (EOS) for NAHS fluid mixtures, which can be straightforwardly applied to polydisperse systems. For positive values of the nonadditivity parameter Δ the model gives accurate predictions of the simulated fluid-fluid coexistence curves and compressibility factors. *NPT* Monte Carlo simulations of the mixing properties of the NAHS symmetric binary mixture with $\Delta>0$ are reported. It is shown that the enthalpy of mixing is largely positive and overcomes the positive entropy of mixing when the pressure is increased, leading to a fluid-fluid phase transition with a lower critical solution pressure. Phase equilibria in polydisperse systems are predicted with the model by using the density moment formalism [P. Sollich *et al.*, Adv. Chem. Phys. **116**, 265 (2001)]. We present predictions of the cloud and shadow curves for polydisperse NAHS systems composed of monodisperse spheres and polydisperse colloid particles. A fixed nonadditivity parameter $\Delta>0$ is assumed between the monodisperse and polydisperse spheres, and a Schulz distribution is used to represent the size polydispersity. Polydispersity is found to increase the extent of the immiscibility region. The predicted cloud and shadow curves depend dramatically on the upper cutoff diameter σ_c of the Schulz distribution, and three-phase equilibria can occur for large values of σ_c.

DOI: 10.1103/PhysRevE.78.021202 PACS number(s): 61.20.−p, 64.75.Cd, 64.10.+h, 64.75.Xc

I. INTRODUCTION

Knowledge of the phase behavior of colloid dispersions is of crucial importance for many applications related to the food, paint, and pharmaceutical industries. Hard-sphere systems are commonly used to represent mixtures of colloidal particles. Additive hard-sphere (AHS) systems are hard-sphere mixtures for which the cross collision diameters σ_{ij} between spheres i and j is equal to the arithmetic mean $\delta_{ij}=(\sigma_{ii}+\sigma_{jj})/2$, while nonadditive hard-sphere system are mixtures where σ_{ij} is different from δ_{ij}. For nonadditive hard-sphere (NAHS) binary mixtures it is common to define a nonadditivity parameter Δ as $\Delta=(\sigma_{12}-\delta_{12})/\delta_{12}$. The case $\Delta=0$ corresponds to an additive binary mixture. Symmetric HS mixtures are binary mixtures of hard spheres of equal sizes ($\sigma_{11}=\sigma_{22}$), while asymmetric mixtures correspond to the cases where σ_{11} differs from σ_{22}. The current work deals with both symmetric and asymmetric NAHS systems, mainly with positive nonadditivities $\Delta>0$. The reader is directed to a paper by Santos *et al.* [1] for a review of the theoretical and simulation studies of NAHS mixtures. Fluid-fluid demixing in nonadditive systems with $\Delta>0$ was clearly observed from molecular simulation [2–4]. This fluid-fluid phase separation can be explained by the fact that the packing of the hard spheres is more difficult in the nonadditive mixture than it is when the unlike species demix. Some prototype NAHS binary mixtures have been studied with great attention, such as the Widom-Rowlinson model system [5]. This system is a symmetric mixture where both hard-sphere components have an infinitely small diameter compared to the positive cross diameter ($\sigma_{11}=\sigma_{22}=0$, $\sigma_{12}>0$). It is one of the simplest model systems that exhibit a fluid-fluid phase transition. The Asakura-Oosawa (AO) model [6] ($\sigma_{11}>0$, $\sigma_{22}=0$, $\sigma_{12}>0$) is another well-known model mixture that has often been used to represent the phase transitions in colloid particles and nonabsorbing polymer mixtures. This model system assumes that the polymer chains (component 2) are ideal chains that can completely overlap ($\sigma_{22}=0$), and takes both the colloid-colloid and polymer-colloid repulsive interactions into account via the diameters σ_{11} and σ_{12}, respectively. Colloid systems are not the only applications of the NAHS model systems. NAHS mixtures may also be employed as the reference systems in equations of state based on perturbation theory and attractive intermolecular potentials. The intuitive combining rule $\sigma_{12}=(\sigma_{11}+\sigma_{22})/2$ corresponding to the additive mixture ($\Delta=0$) is often used to predict the thermodynamic properties of real mixtures, but this is not an exact rule: Δ can significantly deviate from 0 for real systems such as rare gas mixtures. The so-called gas-gas phase transition at high pressure observed in mixtures of rare gases [7] is an example of fluid-fluid phase separation due to the positive nonadditivity of the cross effective diameters. For engineering applications the nonadditivity parameter Δ can be a very useful adjustable parameter to represent phase equilibria data [8].

Real colloid systems are polydisperse. As a polydisperse system contains many different species, a large number of nonlinear equations (corresponding to the equality of the chemical potentials of these species in both phases) must be simultaneously solved for the determination of the phase equilibria. Most equations of state for multicomponent systems can be expressed in terms of a finite number of moments of the distribution function characterizing the size polydispersity, and the phase equilibria problem can be reduced to a few equations. Excellent reviews of the methodologies employed for the calculation of phase equilibria in

*patrice.paricaud@ensta.fr

polydisperse systems can be found in the literature [9–11]. In the case of NAHS systems, accurate equations of state (EOS) were developed to predict the properties of binary mixtures [1,12–20], but none of these equations of state has been applied to a polydisperse NAHS system, to our knowledge. The only studies of the phase equilibria in polydisperse NAHS systems we are aware of are the work of Dickson [21] who used the van der Waals one-fluid mixing rule, and the studies based on the AO model system [22,23]. The aim of the current work is to propose a simple and accurate analytical equation of state for fluid NAHS systems, which considers all components explicitly (i.e., without using any effective potential) and which can be easily extended to polydisperse NAHS mixtures.

This paper is organized as follows: We present an equation of state for NAHS mixtures and evaluate its accuracy by comparing the theoretical predictions to simulation results. We then examine the mixing properties of NAHS mixtures $\Delta > 0$, using both *NPT* Monte Carlo simulations and our EOS, to explain the mechanism of fluid-fluid phase separation in these mixtures. Last, we report predictions of the cloud and shadow curves for a number of polydisperse NAHS systems, and discuss the size fractionation effects and divergence issues when very large diameters are considered.

II. THEORY

A. Equation of state for NAHS mixtures

We consider a multicomponent mixture of N hard spheres in a volume V. The interaction between sphere i of diameter σ_{ii} and sphere j of diameter σ_{jj}, separated by a distance r_{ij}, is described by a hard spherical potential u_{ij} defined as

$$u_{ij} = \begin{cases} +\infty, & r_{ij} \leqslant \sigma_{ij}, \\ 0, & r_{ij} > \sigma_{ij}. \end{cases} \tag{1}$$

The collision diameter σ_{ij} can be nonadditive, i.e., we allow that $\sigma_{ij} \neq (\sigma_{ii}+\sigma_{jj})/2$. The equation of state is based on a first-order perturbation theory that uses the additive hard-sphere mixture as the reference system. The reader is directed to a paper by Adams and McDonald [12] for a comparison between different NAHS models based on perturbation theory. Our equation of state is based on a modification of the MIX1 theory [24,25]. This modification was made to ensure an exact prediction of the second virial coefficients [26]. The model is described as follows: the free energy density f of a multicomponent NAHS mixture, defined as $f=A/V$ where A is the Helmholtz free energy, is given by

$$\frac{f}{kT} = \frac{f^{\mathrm{IDEAL}}}{kT} + \frac{f^{\mathrm{AHS}}}{kT} + \frac{f^{\mathrm{PERT}}}{kT}, \tag{2}$$

where k is the Boltzmann constant, T is the temperature, f^{IDEAL} is the ideal contribution of the free energy density, f^{AHS} is the residual free energy density of the corresponding additive hard-sphere mixture at the same temperature, composition, and density, and f^{PERT} is the perturbation contribution given by [26]

$$\frac{f^{\mathrm{PERT}}}{kT} = \frac{2\pi}{3}\sum_{i,j} \rho_i \rho_j (\sigma_{ij}^3 - \delta_{ij}^3) g_{ij}^{\mathrm{AHS}}, \tag{3}$$

where ρ_i is the number density of sphere i, g_{ij}^{AHS} the contact value of the radial distribution function (RDF) of the ij pair in the additive hard-sphere mixture, and $\delta_{ij}=(\sigma_{ii}+\sigma_{jj})/2$ the additive diameter of the ij pair interaction. The difference between our theory and the MIX1 equation of state [24,25] is the term $(\sigma_{ij}^3-\delta_{ij}^3)$ that replaces the MIX1 term $3\delta_{ij}^2(\sigma_{ij}-\delta_{ij})$. It is clear from Eqs. (2) and (3) that the model correctly predicts the second virial coefficients $B_{ij}=2\pi\sigma_{ij}^3/3$. In Sec. IV A, we show that the term $(\sigma_{ij}^3-\delta_{ij}^3)$ gives rise to better predictions of the simulation data than the MIX1 term. Equation (3) can be expressed in terms of the nonadditivity parameters $\Delta_{ij}=\sigma_{ij}/\delta_{ij}-1$ as

$$\frac{f^{\mathrm{PERT}}}{kT} = \frac{2\pi}{3}\sum_{i,j} \rho_i \rho_j [(1+\Delta_{ij})^3 - 1]\delta_{ij}^3 g_{ij}^{\mathrm{AHS}}. \tag{4}$$

We use the Boublik-Mansoori-Carnahan-Starling-Leland (BMCSL) equation of state [27,28] to calculate the additive contribution f^{AHS}. The BMCSL equation is simple and accurate over a wide range of densities of composition and for large diameter ratios [29]. The contribution f^{AHS} is given by [27,28]

$$\frac{f^{\mathrm{AHS}}}{kT} = \frac{6}{\pi}\left[\left(\frac{\zeta_2^3}{\zeta_3^2} - \zeta_0\right)\ln(1-\zeta_3) + \frac{3\zeta_1\zeta_2}{1-\zeta_3} + \frac{\zeta_2^3}{\zeta_3(1-\zeta_3)^2}\right], \tag{5}$$

where

$$\zeta_l = \frac{\pi}{6}\sum_i^n \rho_i \sigma_{ii}^l. \tag{6}$$

We define the packing fraction η as $\eta=\zeta_3$. The RDF contact values g_{ij}^{AHS} for the additive hard-sphere mixture are consistent with the BMCSL equation of state and are given by [27,28]

$$g_{ij}^{\mathrm{AHS}} = \frac{1}{1-\zeta_3} + \frac{3\sigma_{ii}\sigma_{jj}}{2\delta_{ij}}\frac{\zeta_2}{(1-\zeta_3)^2} + \frac{(\sigma_{ii}\sigma_{jj})^2}{2\delta_{ij}^2}\frac{\zeta_2^2}{(1-\zeta_3)^3}. \tag{7}$$

For the Widom-Rowlinson mixture [5] the free energy density given by the model is equivalent to $f=f^{\mathrm{IDEAL}}+kT\frac{4}{3}\pi\rho_1\rho_2\sigma_{12}^3$, which corresponds to the mean-field solution proposed by Widom and Rowlinson [5].

B. Application to polydisperse NAHS mixtures

We now consider a prototype polydisperse system composed of monodisperse spheres 1 of diameter σ_{11} and polydisperse spheres $i>1$ of diameter σ_{ii}. We suppose that the nonadditive parameters Δ_{ij} between sphere $i>1$ and sphere $j>1$ are equal to zero, i.e., $\sigma_{ij}=\delta_{ij}$ for all $i, j>1$ (the polydisperse spheres are additive between themselves), and that the nonadditivity parameter between a sphere of type 1 and a sphere of type $i>1$ has always the same value Δ, i.e., $\sigma_{1i}=\sigma_{i1}=(1+\Delta)\delta_{1i}$ for all $i>1$. The composition of the polydis-

perse spheres $i>1$ in a given phase is represented by a continuous density distribution ρ_σ defined over the interval $[0,\sigma_c]$, where σ_c is the upper cutoff diameter, i.e., the diameter of the largest sphere in the system; $\rho_\sigma(\sigma)$ is continuous function of σ giving the number density of a spheres of diameter σ in the phase. One can define the lth density moments $\langle\rho_\sigma\rangle_l$ of the diameter distribution ρ_σ as

$$\langle\rho_\sigma\rangle_l = \int_0^{\sigma_c} d\sigma\sigma^l\rho_\sigma(\sigma). \tag{8}$$

The free energy density of the phase is obtained from Eq. (1); the ideal contribution f^{IDEAL} is given by

$$\frac{f^{\mathrm{IDEAL}}}{kT} = \rho_1(\ln\rho_1 - 1) + \int_0^{\sigma_c} d\sigma\rho_\sigma(\sigma)[\ln\rho_\sigma(\sigma) - 1], \tag{9}$$

where ρ_1 is the number density of component 1 (monodisperse spheres of diameter σ_{11}). The de Broglie volumes were removed from Eq. (9) as they do not affect the phase equilibria. The density $\rho=N/V$ of the phase is given by $\rho=\rho_1+\langle\rho_\sigma\rangle_0$. The additive hard-sphere contribution f^{AHS} is given by Eq. (5), where the ζ_l are expressed as

$$\zeta_l = \frac{\pi}{6}(\rho_1\sigma_{11}^l + \langle\rho_\sigma\rangle_l). \tag{10}$$

The perturbation contribution f^{PERT} is obtained from Eq. (4) and is given by

$$\frac{f^{\mathrm{PERT}}}{kT} = \frac{4\pi}{3}\rho_1\int_0^{\sigma_c} d\sigma\rho_\sigma(\sigma)[(1+\Delta)^3 - 1]\left(\frac{\sigma_{11}+\sigma}{2}\right)^3 g_{1\sigma}^{\mathrm{AHS}}, \tag{11}$$

where $g_{1\sigma}^{\mathrm{AHS}}$ is the contact value of the RDF between sphere 1 and a sphere of diameter σ in the additive hard-sphere mixture. The contribution f^{PERT} can be expressed in terms of the density moments $\langle\rho_\sigma\rangle_l$ of the distribution ρ_σ as

$$\begin{aligned}\frac{f^{\mathrm{PERT}}}{kT} = {}& \frac{\pi}{3}\rho_1[(1+\Delta)^3 - 1] \\ & \times\left(\frac{\sigma_{11}^3\langle\rho_\sigma\rangle_0 + 3\sigma_{11}^2\langle\rho_\sigma\rangle_1 + 3\sigma_{11}\langle\rho_\sigma\rangle_2 + \langle\rho_\sigma\rangle_3}{2(1-\zeta_3)}\right. \\ & + \frac{3}{2}(\sigma_{11}^3\langle\rho_\sigma\rangle_1 + 2\sigma_{11}^2\langle\rho_\sigma\rangle_2 + \sigma_{11}\langle\rho_\sigma\rangle_3)\frac{\zeta_2}{(1-\zeta_3)^2} \\ & \left. + (\sigma_{11}^3\langle\rho_\sigma\rangle_2 + \sigma_{11}^2\langle\rho_\sigma\rangle_3)\frac{\zeta_2^2}{(1-\zeta_3)^3}\right).\end{aligned} \tag{12}$$

Since the residual free energy density $f^{\mathrm{RES}}=f-f^{\mathrm{IDEAL}}$ only depends on a finite number of density moments, it belongs to the category of "truncatable" free energies [11,30]. As a result, the number of equations that must be solved for a cloud point calculation does not depend on the number of molecular species. The chemical potential μ_1 of sphere 1 is obtained from the thermodynamic relation $\mu_1=\partial f/\partial\rho_1$. The chemical potential $\mu(\sigma)$ of a sphere of diameter σ is the functional derivative of f with respect to the density distribution $\rho_\sigma(\sigma)$, and is given by

$$\mu(\sigma) = \frac{\delta f}{\delta\rho_\sigma(\sigma)} = kT\ln\rho_\sigma(\sigma) + \sum_{l=0}^{3}\frac{\partial f^{\mathrm{RES}}}{\partial\langle\rho_\sigma\rangle_l}\sigma^l. \tag{13}$$

The pressure of the polydisperse system is obtained from the thermodynamic relation $P=\Sigma\rho_i\mu_i-f$ as [30]

$$P = \rho kT - f^{\mathrm{RES}} + \rho_1\frac{\partial f^{\mathrm{RES}}}{\partial\rho_1} + \sum_{l=0}^{3}\langle\rho_\sigma\rangle_l\frac{\partial f^{\mathrm{RES}}}{\partial\langle\rho_\sigma\rangle_l}\sigma^l. \tag{14}$$

The conditions of the phase equilibria between phases α and β are the equality of the pressure, the equality of the chemical potential of component 1, and the equality of the chemical potential $\mu(\sigma)$ of the spheres of diameter σ in both phases. It can be shown that the latter condition $[\mu^{(\alpha)}(\sigma)=\mu^{(\beta)}(\sigma)]$ is equivalent to [30]

$$\rho_\sigma^{(\beta)}(\sigma) = \rho_\sigma^{(\alpha)}(\sigma)\exp\left[\sum_{l=0}^{3}\left(\frac{\partial f^{\mathrm{RES}(\alpha)}}{\partial\langle\rho_\sigma\rangle_l^{(\alpha)}} - \frac{\partial f^{\mathrm{RES}(\beta)}}{\partial\langle\rho_\sigma\rangle_l^{(\beta)}}\right)\sigma^l\right], \tag{15}$$

where $\langle\rho_\sigma\rangle_l^{(\alpha)}$, $\langle\rho_\sigma\rangle_l^{(\beta)}$ are the lth density moments of the phases α and β. Equation (15) must be satisfied for all values of $\sigma\in[0,\sigma_c]$. At the cloud point, the composition of the cloud phase is equal to the parent composition, and the amount of the shadow phase is infinitely small. Let us assume that phase α is the cloud phase and phase β the shadow phase. For a cloud point calculation it can be shown that the necessary and sufficient conditions for the equality of $\mu(\sigma)$ in both phases for each diameter σ correspond to the definitions of the first four density moments of the shadow phase β [Eq. (8)], i.e.,

$$\begin{aligned}\langle\rho_\sigma\rangle_k^{(\beta)} = {}& \int_0^{\sigma_c} d\sigma\sigma^k\rho_\sigma^{(\alpha)}(\sigma)\exp\left[\sum_{l=0}^{3}\left(\frac{\partial f^{\mathrm{RES}(\alpha)}}{\partial\langle\rho_\sigma\rangle_l^{(\alpha)}}\right.\right. \\ & \left.\left. - \frac{\partial f^{\mathrm{RES}(\beta)}}{\partial\langle\rho_\sigma\rangle_l^{(\beta)}}\right)\sigma^l\right] \quad \text{for } k=0,\ldots,3.\end{aligned} \tag{16}$$

The parent density distribution $\rho_\sigma^{(0)}=\rho_\sigma^{(\alpha)}$ can be expressed as $\rho_\sigma^{(0)}=\langle\rho_\sigma\rangle_0^{(0)}\phi^{(0)}$, where $\langle\rho_\sigma\rangle_0^{(0)}$ is the zero density moment of $\rho_\sigma^{(0)}$, and $\phi^{(0)}$ is the normalized parent distribution defined over $[0,\sigma_c]$, which describes the global composition of the polydisperse spheres in the system. We use a continuous and normalized Schulz distribution for $\phi^{(0)}$, which is given by

$$\phi^{(0)}(\sigma) = \frac{\sigma^{\lambda-1}e^{-b\sigma}}{\int_0^{\sigma_c}d\sigma\sigma^{\lambda-1}e^{-b\sigma}}. \tag{17}$$

One can show that $\lim_{\sigma_c\to+\infty}\int_0^{\sigma_c}\sigma^{\lambda-1}e^{-b\sigma}d\sigma=\Gamma(\lambda)/b^\lambda$. The parameters b and λ characterize the shape of the Schulz distribution: For $\sigma_c\to+\infty$, λ is related to the width of the distribution function via the index of polydispersity $I_p=\langle\rho_\sigma\rangle_2^{(0)}\langle\rho_\sigma\rangle_0^{(0)}/(\langle\rho_\sigma\rangle_1^{(0)})^2$ as $\lambda=1/(I_p-1)$, and b is related to the number average diameter $\langle\sigma\rangle^{(0)}=\langle\rho_\sigma\rangle_1^{(0)}/\langle\rho_\sigma\rangle_0^{(0)}$ as $b=\lambda/\langle\sigma\rangle^{(0)}$. Those relations between λ, b and the moments are nearly correct for large values of σ_c and weak polydispersity indexes I_p. We have determined the cloud and shadow phase for different values of I_p, and different diameter ratios $q=\langle\sigma\rangle^{(0)}/\sigma_{11}$, and observed that the predicted cloud and

shadow curves were very sensitive to the cutoff diameter σ_c (see Sec. IV B). The cloud and shadow points are determined for a fixed parent composition, by solving a system of six nonlinear equations [four equations corresponding to Eq. (16), and two equations corresponding to the equality of the pressure and the equality of μ_1 in both phases]. The six unknowns are the four density moments $\langle \rho_\sigma \rangle_k^{(\beta)}$, $k=0,\ldots,3$ of the shadow phase, and the densities of both phases $\rho^{(\alpha)}$ and $\rho^{(\beta)}$.

III. SIMULATION DETAILS

Standard *NPT* Monte Carlo (MC) simulations of fluid hard-sphere binary mixtures were performed with a total number of spheres $N=500$, at different reduced pressures $P^*=P\sigma_{11}^3/kT$ and compositions. We checked that the finite size effects were negligible by performing Monte Carlo simulations of about 900 spheres: The differences between the average properties obtained with 500 and 900 particles were small and within the standard deviations of the properties. Periodic boundary conditions and minimum image criterion were applied to a cubic simulation box. Translation and volume MC moves were performed with an acceptance ratio of about 30%. As the studied mixtures were not very dense, the reduced chemical potential μ_i of sphere i could be determined with a reasonable accuracy by using the Widom test particle insertion method [31] (TPI). In the *NPT* ensemble μ_i is determined from the following expression [32]:

$$\frac{\mu_i}{kT} = -\ln\left(\frac{1}{N_i+1}\left\langle \frac{V}{\sigma_{11}^3}\psi \right\rangle\right), \tag{18}$$

where V is the instantaneous volume of the simulation box, $\psi=1$ if the inserted particle does not overlap with any over sphere in the box, and $\psi=0$ if there is an overlap. The symbol $\langle\cdots\rangle$ denotes an average over the Monte Carlo simulation. A large number of MC steps were required to obtain a good estimate of the Gibbs free energy of mixing: The properties were averaged over three-million cycles, with one volume move per cycle in average. Once the chemical potentials of all components are determined with the TPI method, the reduced Gibbs energy $G^*=G/NkT$ is obtained from $G^*=\Sigma_i x_i\mu_i/kT$. The reduced enthalpy of the mixture is given by $H^*=H/NkT=P^*\langle V^*\rangle/N$, and the reduced entropy $S^*=S/Nk$ is obtained using $S^*=H^*-G^*$. The reduced properties of mixing $(\Delta G^*,\Delta H^*,\Delta S^*)$ at fixed temperature T and pressure P (fixed reduced pressure P^*) are defined as

$$\Delta G^* = G^* - \sum_i x_i G^*_{i,\text{pure}},$$

$$\Delta H^* = H^* - \sum_i x_i H^*_{i,\text{pure}},$$

$$\Delta S^* = S^* - \sum_i x_i S^*_{i,\text{pure}}, \tag{19}$$

where $G^*_{i,\text{pure}}$, $H^*_{i,\text{pure}}$, and $S^*_{i,\text{pure}}$ are the Gibbs free energy, enthalpy, and entropy of pure component i at the same T and P. The MC simulation data are reported in Table I.

TABLE I. Thermodynamic properties (reduced density $\rho^*=\rho\sigma_{11}^3$ and chemical potentials μ_i/kT) of the symmetric nonadditive hard-sphere binary mixture with $\Delta=0.2$ ($\sigma_{11}=\sigma_{22}$, $\sigma_{12}=1.2\sigma_{11}$) obtained with *NTP* Monte Carlo simulation of 500 spheres at different reduced pressures $P^*=P\sigma_{11}^3/kT$ and for different mole fractions x_1 of component 1.

x_1	ρ^*	μ_1/kT	μ_2/kT
$P^*=0.4$			
0	0.23615	⋯	−0.168
0.1	0.22607	−1.676	−0.259
0.2	0.21982	−1.173	−0.341
0.3	0.21556	−0.921	−0.426
0.4	0.21281	−0.754	−0.524
0.5	0.21194	−0.628	−0.628
$P^*=0.8$			
0	0.35501	⋯	1.183
0.1	0.33586	0.249	1.103
0.2	0.32502	0.596	1.051
0.3	0.31784	0.736	0.995
0.4	0.31410	0.829	0.947
0.5	0.31300	0.895	0.895
$P^*=1.2$			
0	0.43543	⋯	2.199
0.1	0.41035	1.741	2.135
0.2	0.39694	1.935	2.098
0.3	0.38936	1.994	2.076
0.4	0.38506	2.024	2.058
0.5	0.38374	2.043	2.043

IV. RESULTS AND DISCUSSION

A. Binary systems

We first compare the predictions of the equation of state [Eq. (2)–(7)] to the simulation data of NAHS binary mixtures available in the literature [33–35]. We also compare the model to three other NAHS models: The MIX1 approach [24,25] which is based on a first-order perturbation theory from the additive mixture, the van der Waals one-fluid (vdW-1f) mixing rule applied to the Carnahan-Starling equation of state [36] with the effective packing fraction $\eta_{\text{eff}}=\frac{\pi}{6}\rho\Sigma_{i,j}x_ix_j\sigma_{ij}^3$, and the equation of state developed by Santos *et al.* [1]. As shown in Figs. 1 and 2, the model gives excellent predictions of the compressibility factors for a broad range of nonadditivity Δ and for both symmetric and asymmetric NAHS mixtures. For $\Delta\geqslant-0.05$ the model is of comparable accuracy as the equation of state proposed by Santos *et al.* [1]. The model is more accurate than the MIX1 theory [24,25] (Figs. 1 and 2) particularly at low densities (Fig. 3), as it exactly predicts the cross second virial coefficient, while the MIX1 expression depends linearly on the nonadditivity

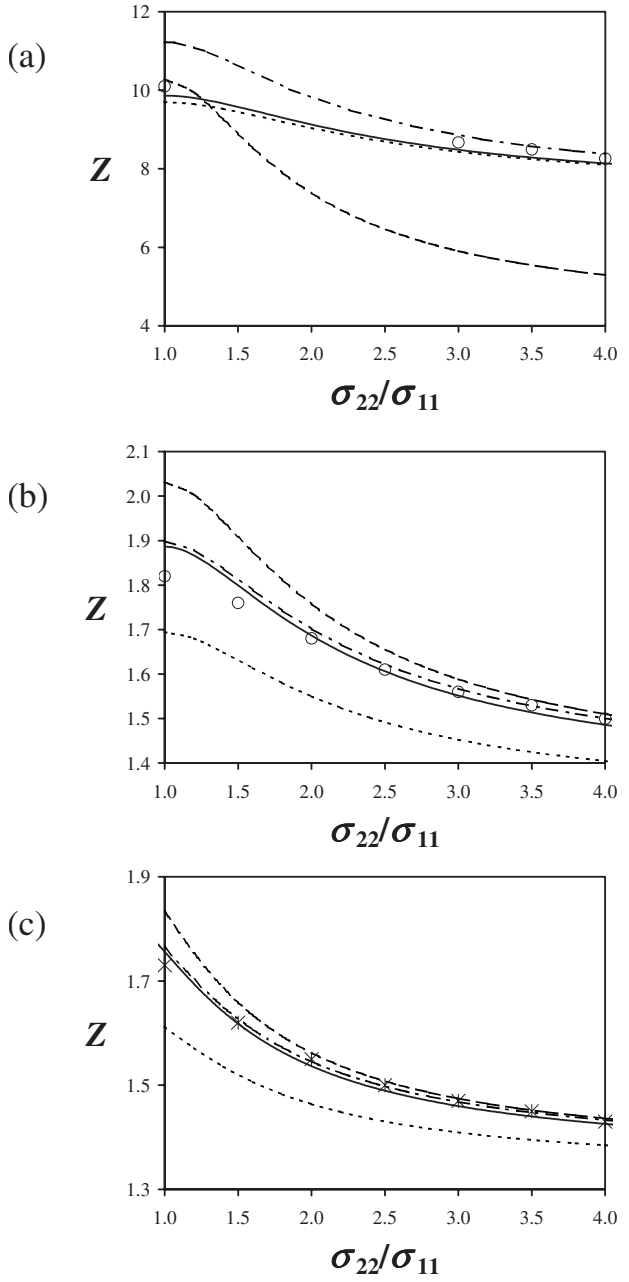

FIG. 1. Compressibility factor of nonadditive hard-sphere binary mixtures as a function of the diameter ratio σ_{22}/σ_{11}, for different values of nonadditivity Δ, packing fraction $\eta=\frac{\pi}{6}\rho(x_1\sigma_{11}^3+x_2\sigma_{22}^3)$ and component 1 mole fraction x_1. (a) $\Delta=-0.05$, $\eta=0.5$; $x_1=0.5$; (b) $\Delta=0.5$, $\eta=0.075$, $x_1=0.5$; (c) $\Delta=0.5$, $\eta=0.075$, $x_1=0.25$. The symbols denote the molecular dynamics simulation data of Hamad [35]. The NAHS equation of state (solid lines) is compared to several NAHS models: The equation of state proposed by Santos *et al.* [1] (dashed-dotted line), the MIX1 theory [24,25] (dotted lines), and the van der Waals one-fluid mixing rule applied with the Carnahan-Starling model [36] (dashed lines).

parameter Δ. The model is clearly more accurate than the vdW-1f model for asymmetric mixtures with $\Delta>0$ [Figs. 1(a) and 2]. Although our model gives reasonably good predictions for moderate negative values of Δ (Fig. 2 and 3) it does not satisfy the limit $\Delta=-1$. In this limiting case, the

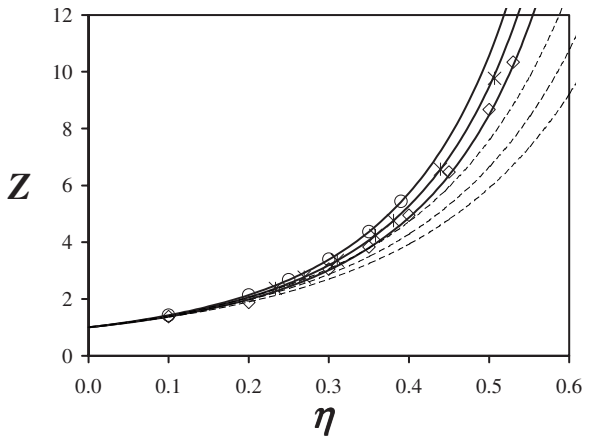

FIG. 2. Compressibility factor of equimolar hard-sphere binary mixtures with a diameter ratio $\sigma_{22}/\sigma_{11}=3$, as a function of the packing fraction $\eta=\frac{\pi}{6}\rho(x_1\sigma_{11}^3+x_2\sigma_{22}^3)$. The symbols denote the molecular dynamics simulation data of Hamad [35]: Circles, $\Delta=0.05$; asterisks, $\Delta=0$; diamonds, $\Delta=-0.05$. The solid lines are the predictions of the current NAHS equation of state. The dashed lines are the predictions of the van der Waals one-fluid mixing rule applied with the Carnahan and Starling equation of state [36]. Here the curves calculated with the MIX1 [24,25] and Santos *et al.* [1] models are not reported as they are similar to the curves calculated with our model.

unlike species do not interact, so the residual free energy of the system is the sum of the residual free energies of the pure species, i.e., $f=f^{\mathrm{IDEAL}}+\Sigma_i f^{\mathrm{AHS}*}(\rho_i,\sigma_{ii})$, where $f^{\mathrm{AHS}*}(\rho_i,\sigma_{ii})$ is the residual free energy density of the pure hard-sphere compound i of diameter σ_{ii} at density ρ_i. The theories [14,15] that exactly satisfy the limit $\Delta=-1$ are more accurate than the current model for large negative values of Δ, particularly at high densities [Fig. 3(a)]. The model of Santos *et al.* [1] does not satisfy this limit either, but remains very accurate for negative values of Δ and high densities [Fig. 3(a)]. The model is reasonably accurate at low densities even for large negative Δ as it correctly predicts the second virial coefficients [Fig. 3(b)], but it becomes unreliable for $\Delta<-0.1$ at high densities [Fig. 3(a)].

The model gives good predictions of the fluid-fluid coexistence curves for NAHS mixtures with $\Delta>0$, except in the near-critical region [Figs. 4, 5, and 6(a)]. The difficulty to represent the near-critical region can be explained by the fact that the current model does not predict the correct critical exponents. For diameter ratios close to 1 (Fig. 4), the coexistent curves calculated with the model are very similar to those obtained with the model of Santos *et al.* [1], but are closer to the simulated data [3] than the curves calculated with the vdW-1f and MIX1 models. The MIX1 model tends to underestimate the immiscibility between the two hard-sphere components, while the vdW-1f model overestimates it. The binodal curves of the asymmetric NAHS binary mixture with $\sigma_{22}/\sigma_{11}=0.1$ have been predicted for different nonadditivities $\Delta>0$ (Fig. 5). The predictions of the MIX1 and vdW-1f models are unsatisfactory: The vdW-1f model largely underestimates the critical pressures for small values of Δ [Fig. 5(b)], while the MIX1 model overestimates them for large values of Δ [Fig. 5(a)]. For pressures higher than

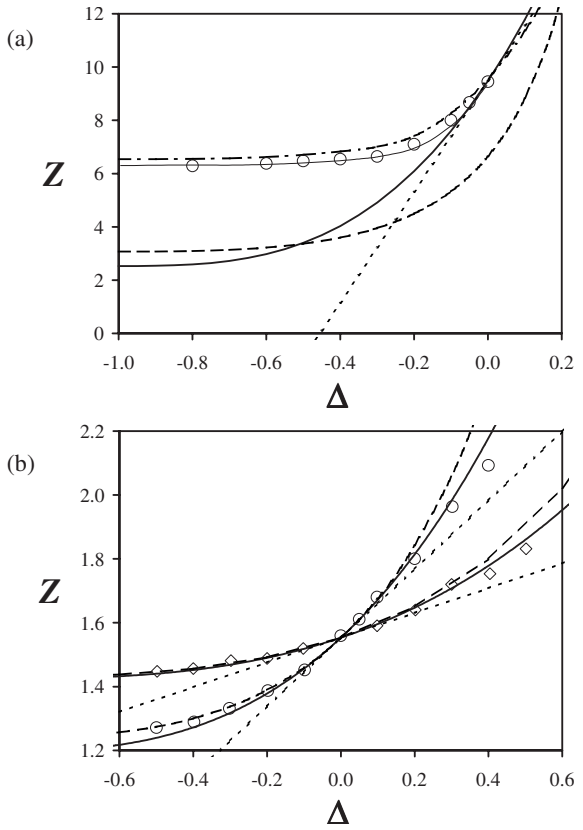

FIG. 3. Compressibility factor of nonadditive hard-sphere binary mixtures as a function of the nonadditivity parameter Δ. (a) Asymmetric NAHS mixture with a diameter ratio $\sigma_{22}/\sigma_{11}=3$ and at packing fraction $\eta=0.5$. The circles denote the simulation data of Hamad [35]. (b) Symmetric NAHS mixture ($\sigma_{11}=\sigma_{22}$) at packing fraction $\eta=\pi/30$. The symbols denote the simulation data of Jung *et al.* [33,34]: The diamonds correspond to $x_1=0.1$, and the circles to $x_1=0.5$. In (a) and (b), the NAHS equation of state (thick solid lines) is compared to several NAHS models: The equation of state proposed by Santos *et al.* [1] (dashed-dotted line), the MIX1 theory [24,25] (dotted lines), and the van der Waals one-fluid mixing rule applied with the Carnahan-Starling model [36] (dashed lines). The thin solid lines are the predictions of Hamad's equation of state based on Eq. (10) of Ref. [35].

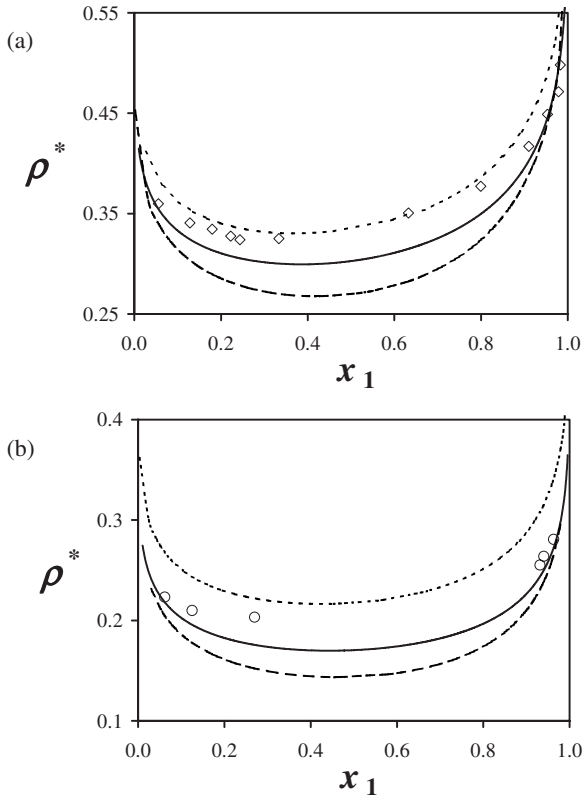

FIG. 4. Fluid-fluid phase separation shown in the density-composition plane for NAHS asymmetric binary mixtures with $\sigma_{22}/\sigma_{11}=1.2$ and different values of σ_{12}. The reduced density is expressed as $\rho^*=\rho\sigma_{11}^3$. The open symbols denote the GEMC simulation data of Rovere and Pastore [3]. (a) Diamonds, $\sigma_{12}=1.3\sigma_{11}$ (i.e., $\Delta\approx 0.181\,82$); (b) Circles, $\sigma_{12}=1.5\sigma_{11}$ (i.e., $\Delta\approx 0.363\,64$). The model (solid lines) is compared to the MIX1 theory [24,25] (dotted lines), and to the van der Waals one-fluid mixing rule applied with the Carnahan-Starling model [36] (dashed lines). The curves calculated with the model developed by Santos *et al.* [1] are not shown here, as they are very similar to those obtained with our model.

the critical points, the current model is more accurate than all of the other tested models, while the Santos *et al.* [1] and the Dijkstra models [4] are more accurate for the prediction of the critical composition [Figs. 5(c) and 5(d)]. The curves calculated with the model of Santos *et al.* [1] are very similar to those obtained with Dijkstra's model [4] based on the Barboy and Gelbart *y* series expansion [4,37], except for the case $\Delta=0.2$. Based on all these comparisons, one can conclude that the current model is more accurate for the MIX1 and vdW-1f approaches and as accurate as the model proposed by Santos *et al.* [1], for positive nonadditivities Δ. One key advantage of the current model is that one can easily express the free energy in terms of the density moments to solve the phase equilibria for a continuous polydisperse system. For negative nonadditivities the model is reliable as long as the density is low. At high density, it gives accurate predictions only for $\Delta>-0.1$ and other NAHS models [1,35] should be used for $\Delta<-0.1$.

We now examine the properties of mixing of the symmetric NAHS mixture at different state conditions, to investigate the driving force for the phase separation. The reduced Gibbs free energy, enthalpy, and entropy of mixing (ΔG^*, ΔH^*, and ΔS^*) of the symmetric NAHS mixture with $\Delta=0.2$ have been determined from density and chemical potential data obtained by *NPT* Monte Carlo simulation (Table I). The mixing properties were simulated at different reduced pressures $P^*=P\sigma^3/kT$ outside but close to the fluid-fluid coexistence region, in order to observe the evolution of these properties when the pressure is increased towards the demixing region. As shown in Fig. 6, the model accurately predicts the mixing properties far from the critical point [Figs. 6(b)–6(d)]. The difficulty to represent the near critical region can also be related to the incorrect predictions of the critical exponents. One can see in Fig. 6(b) that the simulated Gibbs free energy of mixing ΔG^* is negative for the whole composition range, but increases when the pressure P is increased at fixed temperature. The curvature and sign of ΔG^* predicted with the model change when the pressure is higher than the critical

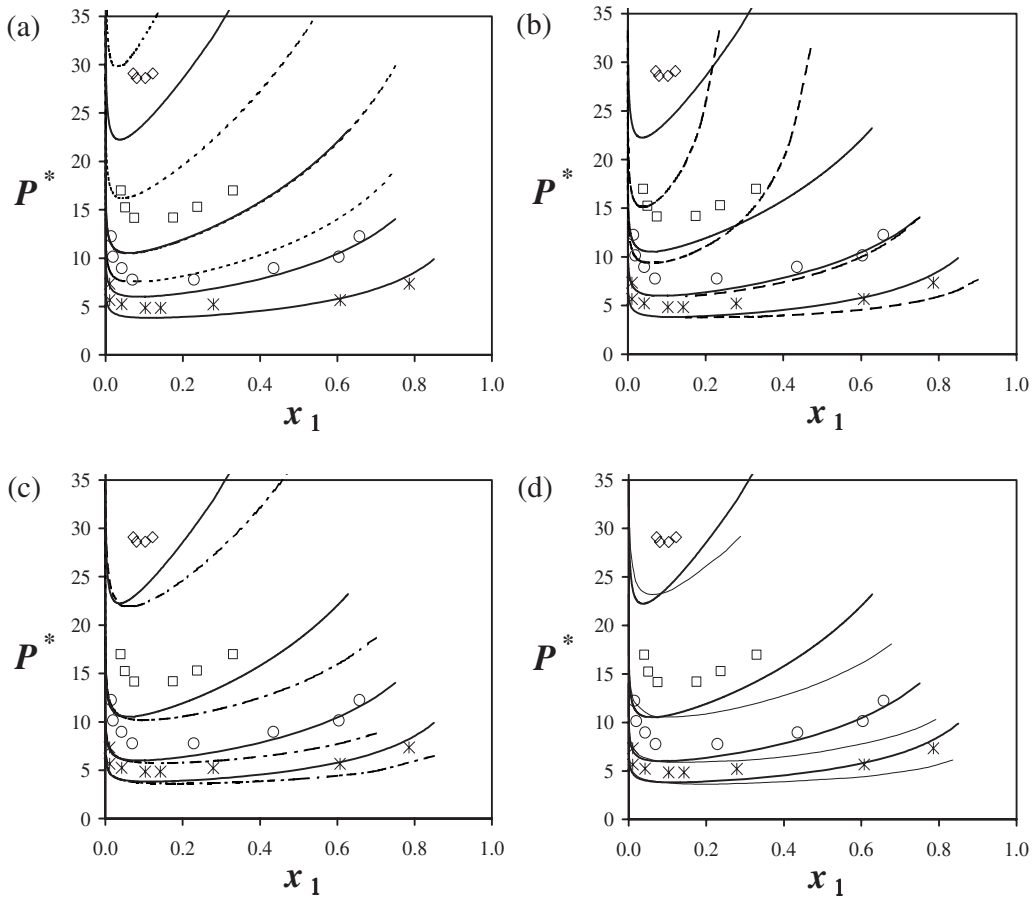

FIG. 5. Fluid-fluid phase separation shown in the pressure-composition plane for NAHS asymmetric binary mixtures with $\sigma_{22}=0.1\sigma_{11}$ and different values of Δ. The reduced pressure is expressed as $P^*=P\sigma_{11}^3/kT$. The open symbols denote the GEMC simulation data of Dijkstra [4]: Asterisks, $\Delta=0.5$; circles, $\Delta=0.4$; squares, $\Delta=0.3$; diamonds, $\Delta=0.2$. The model (thick solid lines) is compared to several other nonadditive hard-sphere models: (a) MIX1 theory [24,25] (dotted lines); (b) van der Waals one-fluid mixing rule applied with the Carnahan-Starling equation of state [36] (dashed-lines); (c) equation of state developed by Santos *et al.* [1] (dashed-dotted lines); (d) Dijkstra's model based on the Barboy and Gelbart y series expansion [4,37] (thin solid lines).

pressure. The curvature of ΔG^* is given by the sign of the second derivative of ΔG^* with respect to x_1, and characterizes the stability of the mixture. Thus, it is clear that the system goes toward a phase transition when the pressure is increased at fixed T. In Fig. 6(c), one can see that the reduced enthalpy of mixing is largely positive and dramatically increases as the pressure is increased. As a result, the enthalpy of mixing clearly favors demixing. The positive sign of ΔH^* comes from the large and positive volume of mixing ($\Delta H^*=P^*\Delta V^*/N$). The entropy of mixing ΔS^* is positive at all of the studied pressures [Fig. 6(d)]. At low pressures the positive entropy of mixing is mainly composed of the ideal entropy of mixing $\Delta S^{*\mathrm{IDEAL}}=-\Sigma_{i=1,2}x_i \ln x_i$, and overcomes the positive enthalpy of mixing ΔH^*. According to the relation $\Delta G^*=\Delta H^*-\Delta S^*$, the Gibbs free energy of mixing at low pressures is negative and concave, and the mixture is stable. As the pressure is increased, the magnitude of ΔS^* decreases due the excess entropy of mixing $S^{*E}=\Delta S^*-\Delta S^{*\mathrm{IDEAL}}$ that is negative and decreases, but the overall ΔS^* remains positive. At higher pressures above the critical point, fluid-fluid demixing occurs as the Gibbs free energy becomes positive and convex due to the positive enthalpy of mixing ΔH^* that overcomes the positive entropy of mixing. Note that a very similar behavior was predicted with the TPT1 theory for mixtures of colloid particles and nonabsorbing polymer chains [38].

B. Polydisperse systems

Phase equilibria have been predicted for a number of prototype polydisperse NAHS systems by using the current equation of state and the methodology described in Sec. II B. The studied polydisperse systems are mixtures of monodisperse spheres of diameter σ_{11} and polydisperse spheres characterized by a parent average diameter $\langle\sigma\rangle^{(0)}$ and a parent polydispersity index I_p. The case $I_p=1$ corresponds to a binary mixture of nonadditive spheres. For $I_p>1$ the parent composition of the polydisperse particles is represented by a Schulz distribution defined over the diameter range $[0, \sigma_c]$, where σ_c is the upper cutoff diameter. The polydisperse spheres are assumed to interact with additive collision diameters, while the cross interactions between the monodisperse and polydisperse particles are nonadditive and characterized by a fixed nonadditivity $\Delta>0$ (see Sec. II B for further details).

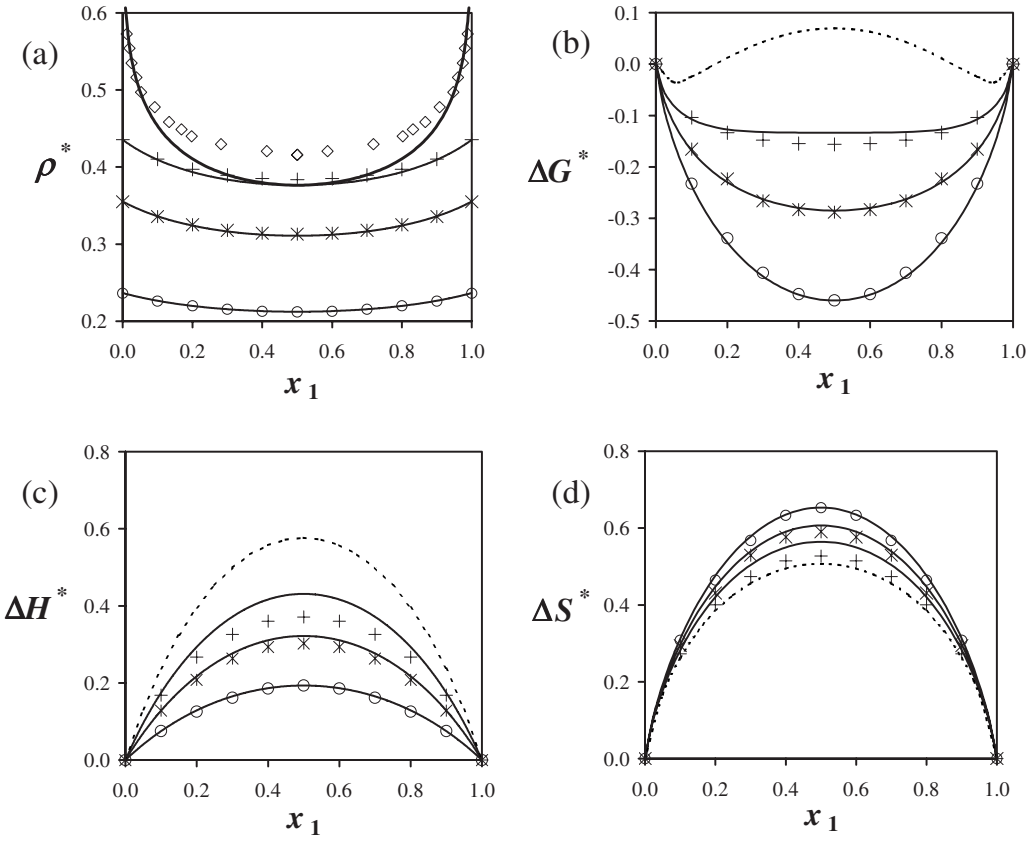

FIG. 6. Reduced thermodynamic properties of mixing of the symmetric nonadditive hard-sphere binary mixture with $\Delta=0.2$ ($\sigma_{11}=\sigma_{22}$, $\sigma_{12}=1.2\sigma_{11}$) as a function of composition and at different reduced pressures ($P^*=P\sigma_{11}^3/kT$). (a) Densities $\rho^*=\rho\sigma_{11}^3$; (b) Gibbs free energy of mixing; (c) enthalpy of mixing; (d) entropy of mixing. In (a), the diamonds denote the simulated fluid-fluid coexistence data obtained by Amar [2], and the thick solid line is the corresponding coexistence curve predicted with our NAHS model. The other symbols denote the *NPT* Monte Carlo simulation data reported in Table I: Circles, $P^*=0.4$; asterisks, $P^*=0.8$; pluses, $P^*=1.2$. The solid lines represent the corresponding predictions of our NAHS model. The dotted lines represent the predicted mixing properties at a pressure $P^*=1.8$ above the critical pressure.

The effect of polydispersity on the phase behavior is shown in Figs. 7–9. In the case of the binary system ($I_p=1$), the compositions of the coexistent phases are given by the binodal curves. For polydisperse systems, the binodal curves of the monodisperse case are replaced by two different curves [Figs. 7(a) and 8]: The cloud and the shadow curve. The cloud curve gives the first pressure where phase separation occurs for a given global (or parent) composition, and the shadow curve gives the composition of the first droplet of the other phase called shadow phase. The critical point of the polydisperse mixture [represented as a circle in Figs. 7(a) and 8] is located at the intersection of the cloud and shadow curves. As the polydisperse index I_p of the parent distribution is increased, the immiscibility region is extended and the critical point is shifted to lower pressures. Note that the enhancement of the fluid-fluid demixing by polydispersity was also observed in colloid-polymer mixtures [22,23,39–41].

The number average diameter of the polydisperse colloids and the diameter distribution in the shadow phase have been determined to examine the size fractionation caused by the phase separation. The average diameter in the shadow phase $\langle\sigma\rangle^{(sh)}$ is larger than the parent average diameter $\langle\sigma\rangle^{(0)}$ when the cloud phase is the component 1 rich phase [Fig. 7(b)]. This means that the largest polydisperse particles remain in the component 1 poor phase, thus, that large spheres are more incompatible with component 1 than small spheres. One can see in Fig. 7(c) that the diameter distribution in the shadow phase is very similar to the parent distribution, however the polydispersity index and the average diameter are different: When the component 1 composition of the cloud phase $x_1^{(cl)}$ is higher than the critical composition x_c, the distribution in the shadow phase is wider (larger polydispersity index) than the parent distribution, while it is narrower for $x_1^{(cl)}<x_c$. Moreover, the predicted cloud and shadow curves depend a lot on the upper cutoff diameter σ_c. When the cutoff σ_c is increased, the cloud and shadow curves are shifted to lower pressures. We observe that some parts of the cloud curve do not converge when the cutoff σ_c tends to infinity. Such a behavior was not observed in mixtures of polydisperse polymers and monodisperse colloid particles [40]: In the case of the polydisperse polymer and monodisperse colloid mixture, the predicted cloud and shadow curves converge for parent Schulz distributions with $\sigma_c\to+\infty$, and the results do not depend on σ_c as long as σ_c is large [40]. It was actually shown for these mixtures that the distribution function in the shadow phase is also a Schulz distribution [40]. For the polydisperse NAHS system the cloud curves can di-

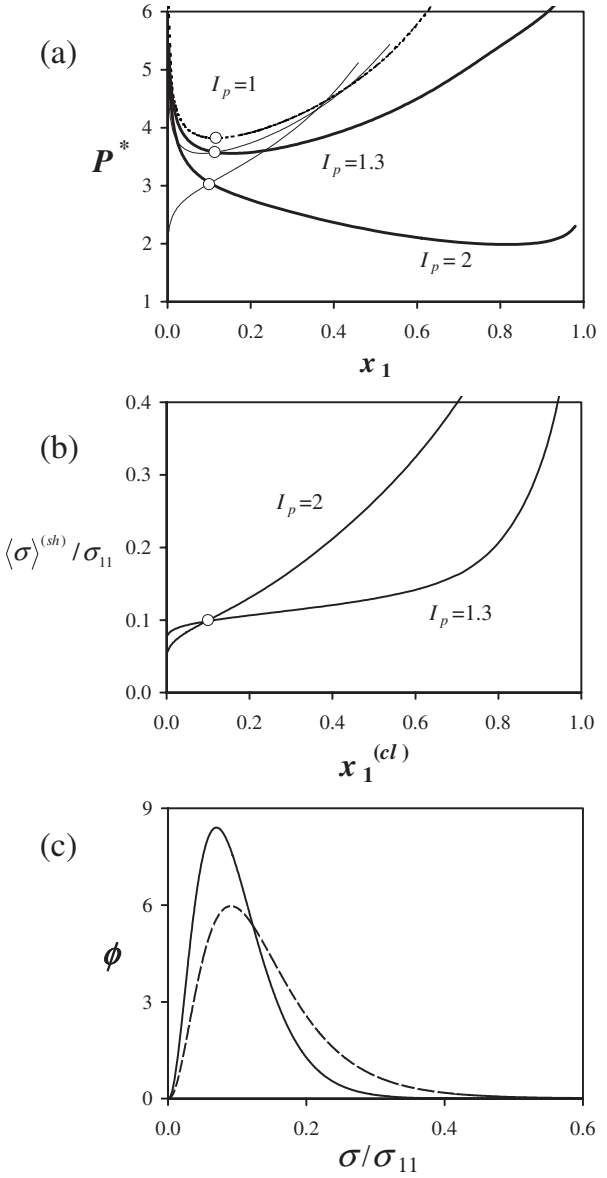

FIG. 7. Effect of polydispersity on the phase behavior of asymmetric NAHS mixtures. The studied polydisperse systems are mixtures of monodisperse spheres (component 1) of diameter σ_{11} and polydisperse spheres with a parent number average diameter $\langle\sigma\rangle^{(0)}=0.1\sigma_{11}$. The monodisperse and polydisperse spheres interact via a fixed nonadditivity $\Delta=0.5$. The size distribution is represented by a Schulz distribution defined over $[0,\sigma_c]$, where $\sigma_c=\sigma_{11}$. Different parent polydispersity indexes are considered ($I_p=1$, $I_p=1.3$, and $I_p=2$). (a) Pressure-composition diagram. The reduced pressure is defined as $P^*=P\sigma_{11}^3/kT$. The dotted curves represent the binodals of the monodisperse NAHS binary mixture with diameter ratio $q=0.1$ and nonadditivity $\Delta=0.5$. The thick and solid lines are the predicted cloud curves and the thin lines are the corresponding shadow curves. The circles denote the predicted critical points. (b) Number average diameter in the shadow phase as a function of the composition in the cloud phase. The circles denote the predicted critical points. (c) Normalized size distribution functions in the cloud and shadow phases predicted at $x_1^{(cl)}=0.6$ with a parent polydispersity index $I_p=1.3$. The solid line represents the parent (cloud phase) diameter distribution and the dashed line represents the diameter distribution in the shadow phase.

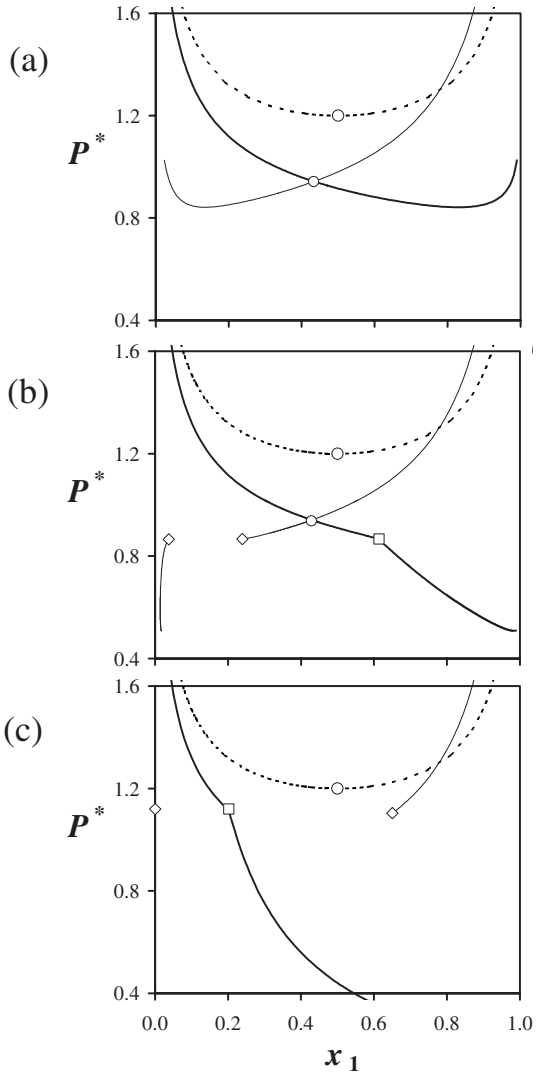

FIG. 8. Effect of the upper cutoff diameter σ_c on the cloud and shadow curves of a NAHS polydisperse mixture. The studied polydisperse system is a mixture of monodisperse spheres (component 1) of diameter σ_{11} and polydisperse particles with a parent number average diameter $\langle\sigma\rangle^{(0)}=\sigma_{11}$, and a parent polydispersity index $I_p=1.1$. The monodisperse and polydisperse spheres interact via a fixed nonadditivity $\Delta=0.2$. The size distribution is represented by a Schulz distribution defined over $[0,\sigma_c]$. Different upper cutoff diameters σ_c are used: (a) $\sigma_c=3\sigma_{11}$, (b) $\sigma_c=5\sigma_{11}$, (c) $\sigma_c=10\sigma_{11}$. The reduced pressure is defined as $P^*=P\sigma_{11}^3/kT$. The dotted curves represent the binodals of the monodisperse and symmetric NAHS binary mixture with $\Delta=0.2$. The thick and solid lines are the predicted cloud curves and the thin lines are the corresponding shadow curves. The circles denote the predicted critical points and the squares indicate the triple points on the cloud curves. The diamonds denote the compositions of the shadow phases at the triple point.

verge when $\sigma_c\to+\infty$. The convergence of the cloud curve is related to the convergence of the integrals in Eq. (16), which depends on the sign of the term $a=(\partial f^{\mathrm{RES}(\alpha)}/\partial\langle\rho_\sigma\rangle_3^{(\alpha)}-\partial f^{\mathrm{RES}(\beta)}/\partial\langle\rho_\sigma\rangle_3^{(\beta)})$ inside the exponential term: The integrals diverge if $a>0$. The condition for convergence also depends on the mathematical form of the parent distribution: The Schulz distribution contains the exponential term $\exp(-b\sigma)$

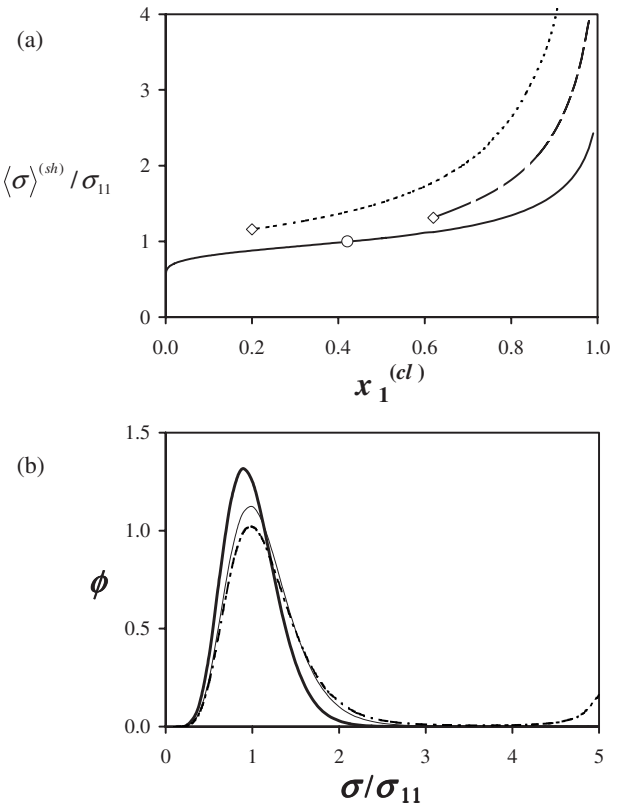

FIG. 9. (a) Effect of the upper cutoff diameter σ_c on the composition of the shadow phase. The studied polydisperse system is the same as in Fig. 8 ($\langle\sigma\rangle^{(0)}=\sigma_{11}$, $I_p=1.1$, $\Delta=0.2$). (a) Number average diameter in the shadow phase as a function of the composition in the cloud phase, obtained with different upper cutoff diameters σ_c: Solid line, $\sigma_c=3\sigma_{11}$; dashed line, $\sigma_c=5\sigma_{11}$; dotted line, $\sigma_c=10\sigma_{11}$. The circle denotes the critical point (composition x_c). For compositions less than the triple-point composition the average diameters in the shadow phase corresponding to $\sigma_c=5\sigma_{11}$ and $\sigma_c=10\sigma_{11}$ are indistinguishable from the average diameters for $\sigma_c=3\sigma_{11}$. The diamonds indicate the compositions of the cloud phase at the triple point for $\sigma_c=5\sigma_{11}$ and $\sigma_c=10\sigma_{11}$. (b) Normalized diameters distribution functions in the three coexistent phases (one cloud and two shadow phases) at the triple-point composition ($x_{tp}\approx 0.62$), for the case $\sigma_c=5\sigma_{11}$. The thick solid line represents the diameter distribution in the cloud phase (parent distribution). The thin solid line represents the diameter distribution in the shadow phase with $x_1^{(cl)}=x_{tp}^-$ (component 1 rich shadow phase), and the dashed-dotted line represents the diameter distribution in the other shadow phase with $x_1^{(cl)}=x_{tp}^+$ (component 1 poor shadow phase).

that converges when $\sigma\to+\infty$, but this term becomes negligible compared to the term $\exp(a\sigma^3)$ in Eq. (16). The divergence of the integrals in Eq. (16) could be avoided by using another parent distribution containing a convergent term such as $\exp(-b\sigma^3)$, with $b>a$.

The increase of σ_c can also lead to three-phase equilibria: As σ_c is increased, a break point (denoted as a square in Fig. 8) can be clearly observed on the cloud curve in the component 1 rich region. This point is a triple point where three-fluid phases are in coexistence. The reader is directed to Ref. [42] for a discussion about such triple points in polydisperse systems. The three-phase point is also characterized by a discontinuity in the shadow curve, which is denoted by two diamonds in Fig. 8(b). This discontinuity shows that the same cloud phase coexist with two types of shadow phases at the triple point. We observed that the branches of the cloud and shadow curves that correspond to cloud phase compositions x_1 below the triple-point composition x_{tp} do not depend on the cutoff diameter σ_c, while the other branches corresponding to $x_1>x_{tp}$ dramatically depend on σ_c (Fig. 8). As σ_c is increased, the critical composition x_c does not significantly change, while the triple-point composition x_{tp} is shifted to lower compositions x_1 [Fig. 8(b)], until the critical point becomes metastable ($x_{tp}<x_c$) for very large cutoffs [Fig. 8(c)].

The average diameter $\langle\sigma\rangle^{(sh)}$ in the shadow phase as a function of the cloud phase composition $x_1^{(cl)}$ is depicted in Fig. 9(a) for the polydisperse symmetric mixture with $\Delta=0.2$. For a short cutoff diameter ($\sigma_c=3\sigma_{11}$) no triple point is observed and the curve $\langle\sigma\rangle^{(sh)}$ vs $x_1^{(cl)}$ is continuous. For large cutoffs ($\sigma_c=5$, $\sigma_c=10$) a triple point appears, and the curve $\langle\sigma\rangle^{(sh)}$ vs $x_1^{(cl)}$ is discontinuous as the cloud curve can coexist with two types of shadow curves. The diamonds in Fig. 9(a) denote the triple-point composition of the cloud curve and the corresponding average diameter $\langle\sigma\rangle^{(sh)}$ in the shadow phase for $\sigma_c=5$ and $\sigma_c=10$. Using Eq. (15), we have determined the diameter distribution functions of the coexistent phases at the triple point for the same polydisperse mixture with $\sigma_c=5$. For this system the cloud phase composition at the triple point is around $x_{tp}\approx 0.62$. The parent Schulz distribution and the distributions of both shadow phases at $x_1^{(cl)}=x_{tp}$ are depicted in Fig. 9(b). One can observe that all distributions are similar in shape for small values of σ, but the distribution in the shadow phase corresponding to the branch $x_1^{(cl)}>x_{tp}$ [represented as a dashed line in Fig. 9(b)] exhibits a second peak near $\sigma=\sigma_c$. This second peak can be mathematically explained by the divergence of the exponential term $\exp(\cdots+a\sigma^3)$ in Eq. (15) when $\sigma\to+\infty$.

It is interesting to compare our results with those obtained by Wilding *et al.* [43,44] for polydisperse spherical particles interacting via Lennard-Jones (LJ) potentials, along the vapor-liquid equilibria curve. Wilding *et al.* [44] found that the diameter distribution in liquid shadow phases in coexistence with vapor cloud phases exhibited a second peak near σ_c, which is very similar to the peak that we find for the NAHS system. To make an analogy between the NAHS mixture and the LJ systems studied by Wilding *et al.* [44], let us consider that the NAHS mixture of component 1 and polydisperse particles can be matched to an effective polydisperse mixture of the same polydisperse particles without component 1, interacting via effective depletion potentials [45]. These effective depletion potentials would take into account the nonadditivity between component 1 and the polydisperse spheres, and contain an attractive part, as the presence of component 1 induces an effective attraction between the polydisperse particles. We can then relate the LJ and NAHS systems by relating the vapor cloud phases of the LJ system to the cloud phases poor in polydisperse particles in the NAHS system, and the liquid shadow phases of the LJ system to the shadow phases rich in polydisperse particles. According to Wilding *et al.* [44], the appearance of a second peak near σ_c in the shadow phase distribution is due to the

fact that the attractive interactions between the largest LJ spheres are more important, and that the enhancement of their concentration in the shadow phase results from a large free energy gain. In the case of the NAHS mixture, the effective depletion potentials between the large particles are more attractive, since the largest polydisperse particles are the most incompatible with component 1. Thus, our results are consistent with the findings of Wilding *et al.* [44].

V. CONCLUSION

We propose an analytical equation of state for nonadditive hard-sphere mixtures, which is based on a perturbation from the additive mixture and on a modification of the MIX1 theory. For fluid phases and positive nonadditivities the model is as accurate as the currently available equations of state, and its simple mathematical form makes possible the treatment of continuous polydisperse systems. It is shown from Monte Carlo simulations and theoretical predictions that the enthalpy of mixing is largely positive and overcomes the positive entropy of mixing at high pressures, leading to a fluid-fluid phase separation that ends at a lower critical solution pressure. The density moment formalism is employed to determine the cloud and shadow curves of a number of polydisperse NAHS systems. The studied polydisperse systems are mixtures of monodisperse and polydisperse spheres, which interact with a fixed nonadditivity. The cloud and shadow curves depend a lot on the upper cutoff σ_c of the parent diameter distribution, and three-phase equilibria can be observed for larges values of σ_c. Some similarities are found between the polydisperse NAHS mixtures and the polydisperse LJ systems studied by Wilding *et al.* [43,44]; in particular, the cloud and shadow curves depend a lot on the upper cutoff diameter of the Schulz distribution, and two different peaks can appear in the diameter distribution of the shadow phase.

The current NAHS model cannot only be used to predict the phase behavior of colloid systems, but can also be implemented into engineering equations of state based on perturbation theory to treat real systems such as mixtures of rare gases. The use of the NAHS mixture as the reference system then enables the introduction of an adjustable cross interaction parameter that characterizes the nonadditivity of the repulsive cores.

ACKNOWLEDGMENTS

The author thanks S. Varga, C. Coquelet, and M. S. Zabaloy for interesting discussions that led to this work.

[1] A. Santos, M. López de Haro, and S. B. Yuste, J. Chem. Phys. **122**, 024514 (2005).
[2] J. G. Amar, Mol. Phys. **67**, 739 (1989).
[3] M. Rovere and G. Pastore, J. Phys.: Condens. Matter **6**, A163 (1994).
[4] M. Dijkstra, Phys. Rev. E **58**, 7523 (1998).
[5] B. Widom and J. S. Rowlinson, J. Chem. Phys. **52**, 1670 (1970).
[6] S. Asakura and F. Oosawa, J. Chem. Phys. **22**, 1255 (1954).
[7] J. A. Schouten, Phys. Rep. **172**, 33 (1989).
[8] A. H. Harvey and J. M. Prausnitz, Fluid Phase Equilib. **48**, 197 (1989).
[9] R. L. Cotterman and J. M. Prausnitz, in *Kinetic and Thermodynamic Lumping of Multicomponent Mixtures*, edited by G. Astarita and S. I. Sandler (Elsevier, Amsterdam, 1991).
[10] D. Browarzik and H. Kehlen, in *Equations of State for Fluids and Fluid Mixtures*, edited by J. V. Sengers, R. F. Kayser, C. J. Peters, and H. J. White (Elsevier, Amsterdam, 2000), Vol. 2.
[11] P. Sollich, J. Phys.: Condens. Matter **14**, R79 (2002).
[12] D. J. Adams and I. R. McDonald, J. Chem. Phys. **63**, 1900 (1975).
[13] D. Gazzillo, J. Chem. Phys. **95**, 4565 (1991).
[14] E. Z. Hamad, J. Chem. Phys. **105**, 3229 (1996).
[15] E. Z. Hamad, J. Chem. Phys. **107**, 6877 (1997).
[16] M. Dijkstra, R. vanRoij, and R. Evans, Phys. Rev. E **59**, 5744 (1999).
[17] A. Y. Vlasov and A. J. Masters, Fluid Phase Equilib. **212**, 183 (2003).
[18] K. Jagannathan, G. Reddy, and A. Yethiraj, J. Phys. Chem. B **109**, 6764 (2005).
[19] G. Pellicane, C. Caccamo, P. V. Giaquinta, and F. Saija, J. Phys. Chem. B **111**, 4503 (2007).
[20] P. Sillren and J.-P. Hansen, Mol. Phys. **105**, 1803 (2007).
[21] E. Dickinson, Chem. Phys. Lett. **66**, 500 (1979).
[22] M. Fasolo and P. Sollich, J. Chem. Phys. **122**, 074904 (2005).
[23] M. Fasolo and P. Sollich, J. Phys.: Condens. Matter **17**, 797 (2005).
[24] T. W. Melnyk and B. L. Sawford, Mol. Phys. **29**, 891 (1975).
[25] H. M. Schaink and C. Hoheisel, J. Chem. Phys. **97**, 8561 (1992).
[26] P. Paricaud, J. Chem. Phys. **124**, 154505 (2006).
[27] T. Boublík, J. Chem. Phys. **53**, 471 (1970).
[28] G. A. Mansoori, N. F. Carnahan, K. E. Starling, and T. W. Leland, J. Chem. Phys. **54**, 1523 (1971).
[29] G. Jackson, J. S. Rowlinson, and F. vanSwol, J. Phys. Chem. **91**, 4907 (1987).
[30] P. Sollich, P. B. Warren, and M. E. Cates, Adv. Chem. Phys. **116**, 265 (2001).
[31] B. Widom, J. Chem. Phys. **39**, 2808 (1963).
[32] D. Frenkel and B. Smit, *Understanding Molecular Simulation* (Academic, London, 1996).
[33] J. Jung, M. Jhon, and F. H. Ree, J. Chem. Phys. **100**, 528 (1994).
[34] J. Jung, M. Jhon, and F. H. Ree, J. Chem. Phys. **100**, 9064 (1994).
[35] E. Z. Hamad, Mol. Phys. **91**, 371 (1997).
[36] N. F. Carnahan and K. E. Starling, J. Chem. Phys. **51**, 635 (1969).
[37] B. Barboy and W. M. Gelbart, J. Chem. Phys. **71**, 3053 (1979).

[38] P. Paricaud, S. Varga, and G. Jackson, J. Chem. Phys. **118**, 8525 (2003).
[39] R. P. Sear and D. Frenkel, Phys. Rev. E **55**, 1677 (1997).
[40] P. Paricaud, S. Varga, P. T. Cummings, and G. Jackson, Chem. Phys. Lett. **398**, 489 (2004).
[41] Y. V. Kalyuzhnyi and P. T. Cummings, Chem. Phys. Lett. **443**, 243 (2007).
[42] P. Paricaud, A. Galindo, and G. Jackson, J. Chem. Phys. **127**, 154906 (2007).
[43] N. B. Wilding, P. Sollich, and M. Fasolo, Phys. Rev. Lett. **95**, 155701 (2005).
[44] N. B. Wilding, P. Sollich, M. Fasolo, and M. Buzzacchi, J. Chem. Phys. **125**, 014908 (2006).
[45] R. Roth, R. Evans, and A. A. Louis, Phys. Rev. E **64**, 051202 (2001).